73rd International Astronautical Congress (IAC), Paris, France, 18-22 September 2022.


IAC-22- D2.5.6

# CFD analysis of interaction effects between vehicles in formation flight for in-air capturing of reusable launchers

**Yakut Cansev Kucukosman [a]*, Sophia Buckingham [a], Silvania Lopes [a], Philippe Planquart [a]**

**Sunayna Singh [b], Sven Stappert [b], Leonid Bussler [b], Martin Sippel [b]**

[a] *von Karman Institute for Fluid Dynamics VKI, 72 Chaussée de Waterloo, Rhode-St-Genèse B-1640, Belgium,* yakut.cansev.kucukosman@vki.ac.be
[b] *DLR Institut für Raumfahrtsysteme, Linzer Straße 1, 28359, Bremen, Germany,* sunayna.singh@dlr.de
* Corresponding Author

**Abstract**

Reusing the complex, high performance, high-cost rocket stages and engines by returning them back to their launch site is becoming important not only from economical aspects but also from an ecological point of view. An innovative return mode, 'in-air capturing (IAC)', is chosen as it provides potential for a better performance by reducing the overall fuel consumption, when compared to other approaches like vertical landing. In this mode, a winged reusable launcher vehicle (RLV), which has slowed down to subsonic velocity through atmospheric braking is captured using an aircraft and towed back to launch site. First, the vehicles approach each other in a parallel formation with similar velocities by keeping a safe distance between them. During this formation, a capturing device autonomously captures the RLV. Once the connection has been achieved, the captured configuration is pulled up from a gliding flight to cruise flight with a towing aircraft serving as an external propulsion system to the RLV. During these phases, the RLV is exposed to the wake of the towing aircraft and will face disturbances that will likely lead to a reduction in formation envelope. The impact of proximity between the capturing device and the RLV should also be evaluated to investigate the complex interactions which would alter the aerodynamic performances of both vehicles after connection. Moreover, in the next phase, the connected configuration must pull-up from a descent to cruise flight. For this the towing aircraft will be at high angle of attacks leading to strong downwash velocity in the wake that must be studied further. In this work, a full-scale three-dimensional RANS simulation will be performed with the open source CFD code OpenFOAM 6.0 using the k-ω SST turbulence model and a compressible solver rhoSimpleFoam to investigate aforementioned issues. The CFD results will be analysed to gain better insight in the flow field and interaction effects between the three vehicles and their aerodynamic performance used for the flight dynamics simulation of IAC.

**Keywords:** FALCon, In-Air-Capturing, Reusable Launch Vehicle, Vertical Launch Horizontal Landing, Computational Fluid Dynamics, RANS

**Acronyms/Abbreviations**

| | |
|---|---|
| 3STO | Three Stage To Orbit |
| 3D | Three Dimensional |
| AoA | Angle of Attack |
| ACCD | Aerodynamically Controlled Capturing Device |
| CFD | Computational Fluid Dynamics |
| IAC | In-Air-Capturing |
| L/D | Lift-to-Drag |
| MECO | Main Engine Cut-Off |
| RANS | Reynolds-Averaged Navier Stokes |
| RLV | Reusable Launch Vehicle |
| TA | Towing Aircraft |
| VTVL | Vertical Take-off Vertical Landing |
| VTHL | Vertical Take-off Horizontal Landing |

## 1. Introduction

The demand for the reusability of high performance, high cost rocket stages and other parts like engines is rising with increase in launch frequencies. Several innovative partial and full-recovery methods are being developed to ensure that more and more parts of the launch system are reused. The commonly used methods can be categorized as Vertical Take-off Vertical Landing (VTVL) and Vertical Take-off Horizontal Landing (VTHL). The first approach, which is operated by successful pioneers such as SpaceX and Blue Origin, requires significant fuel consumption during landing [1]. The second method based on winged RLVs can only glide back when there is sufficient energy (descending from orbit), while the ones powered by turbofans requires additional propulsion system which adds to stage mass [1, 2]. An innovative approach called 'In-Air-Capturing (IAC)' patented by DLR overcomes these challenges by

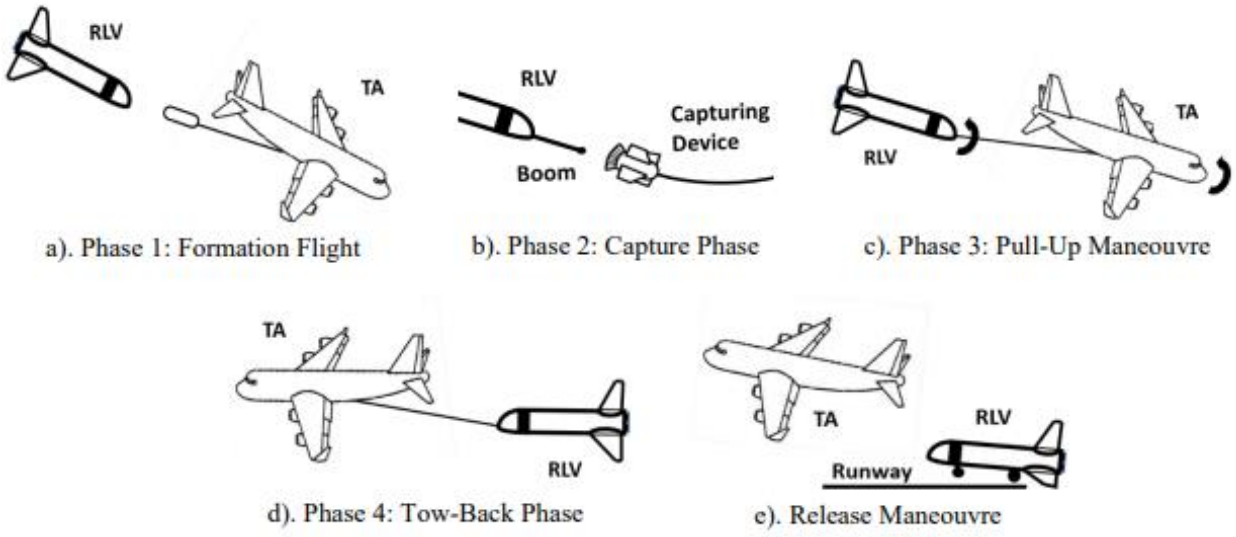


Fig. 1: Phases of In-Air Capturing Manoeuvre [2].

eliminating the additional need for a propulsion system which reduces the associated costs [3].

The operational cycle of a mission with IAC starts with the launcher lifting off vertically and ascending until Main Engine Cut-Off (MECO). At MECO, the winged first stage separates from the launch vehicle and re-enters the atmosphere in a ballistic trajectory, in the course of which it decelerates from supersonic velocity to a subsonic glide. Meanwhile, a capturing aircraft is waiting at the downrange rendezvous area, loitering until the RLV arrives. Between 8 km to 2 km altitude, the final IAC manoeuvre is performed [4]. To understand better the IAC manoeuvre, the process can be divided into five phases as shown in Fig. 1 [2]:

- *Phase 1: Formation Flight* During the formation flight phase (Figure 1a), the Towing Aircraft (TA) glides from cruise flight and attempts to achieve a parallel descending formation with the RLV. Here, both vehicles attempt to maintain similar velocities and flight path angles, while separated by a safe distance. The formation envelope must be maintained long enough for the capture phase to be successfully completed [2]. A detailed analysis of the dynamics and trajectories of this phase can be found in [1].
- *Phase 2: Capture Phase* While the two vehicles are in formation, the capture phase (Figure 1b) is carried out. A capturing device attached to a rope is first released from the aircraft. This agile device autonomously navigates its way to the RLV and ensures mating of the two vehicles. Once the RLV is connected to the TA via the rope, the aircraft acts like an external propulsion system to the RLV. A detailed modelling of critical aspects like aerodynamics, rope dynamics and control architecture of this phase has been discussed in [5], [6] and [2].
- *Phase 3: Pull-Up Manoeuvre* Next the mated configuration in descending flight performs a pull-up manoeuvre (Figure 1c) to transition to an ascending flight. During this, the TA engines are turned on to provide thrust to the system. The configuration can then gain altitude and achieve a suitable cruise state [7].
- *Phase 4: Tow-Back Phase* The tow-back flight (Figure 1d) simply involves the TA towing the RLV to the landing site. The configuration flies at an optimal altitude and velocity to minimize fuel consumption.
- *Phase 5: Release Manoeuvre* The release manoeuvre (Figure 1e) involves release of the RLV by the TA close to the runway. The RLV lands horizontally onto the landing strip using its own landing gear.

As the RLV will be exposed to the wake of the TA during these phases, it is important to investigate the disturbances it causes which may result in reducing the formation flight envelope. Moreover, it is important to analyse the interaction between the two vehicles (ACCD and RLV) to assess the aerodynamic performance after matching. Lastly, at high AoA during the pull-up manoeuvre, a strong downwash velocity component is observed [8], which will change the aerodynamic performance of both vehicles requiring a further analysis. To address the aforementioned issues, a full-scale three-dimensional (3D) simulation needs to be performed. However,

simulating the flow-field around all three vehicles (TA, ACCD and RLV) will result in a high computational cost. Therefore, a two-stage simulation approach is proposed in which the TA is simulated alone to obtain the wake field that is then imposed as an inlet boundary condition to recreate the resulting inflow velocity deficit as well as the turbulent properties. For the simulations, 3D RANS simulations are performed with the open source CFD code OpenFOAM 6.0 using the k-ω SST turbulence model and the compressible solver rhoSimpleFoam.

This paper describes the 3D simulation performed to investigate the interactions between the full-scale vehicles that are performing the IAC manoeuver. The selected full-scale configurations are described in Sec. 2. Later, the wake disturbance from the TA is presented and analysed and its effect on the formation flight is evaluated in Sec. 3. The computational settings of the coupled RLV and ACCD are provided in Sec. 4, 5 and 6. The results and discussion parts are held on Sec. 7 with the conclusions in Sec. 8.

## 2. Selected configurations for full scale simulation

During the parallel formation of IAC, it is required to have both participating vehicles (TA and RLV) to be in a gliding flight by maintaining similar altitudes, velocities and flight path angles separated by a safe distance. To achieve this, it is crucial for both vehicles to reach a similar aerodynamic performance in terms of Lift to Drag ratio (L/D). The following section explains the selected full-scale test cases and the modifications which are needed to reduce the gap between L/D ratios for the formation flight [5]:

- **Reusable Launch Vehicle (RLV):** As the L/D ratios of the commercial aircraft are higher, the L/D ratio of the launcher must be maximised to allow a successful formation. A higher L/D ratio is usually obtained by increasing the wing span and size which in turn decreases the payload capability. As a compromise, a swept wing configuration is proposed and the first stage for a 3 Stage-To-Orbit (3STO) launch vehicle (more details can be found in [9]) is selected and shown in Fig. 2. The stage mass during the descent is approximated to be about 80 tons [5].
- **Towing Aircraft (TA):** Based on the thrust requirements for towing a large RLV stage, a four engine, long range jetliner like the A340-600 was deemed fit [10] (shown in Fig. 3). The retired aircraft comes with powerful Rolls Royce Trent 556 engines and large loading capacity to support the towing loads [1]. In this paper, the TA configuration is selected to have the front and side landing gear as well as the spoilers at 20° deployed to match the L/D ratio of the RLV. Moreover, the engines are selected as CFM56.

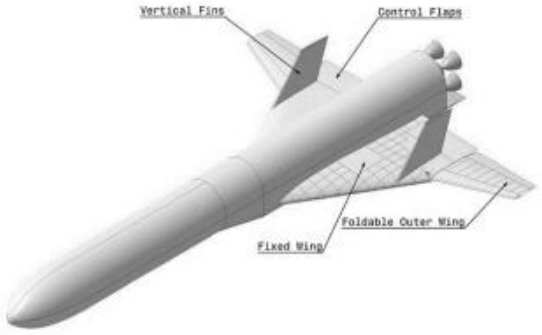


Fig. 2: Subsonic Configuration of RLVC4 [2].

Fig. 3: Commercial Airliner: A340-600 [11].

- **Aerodynamically Controlled Capturing Device (ACCD):** This device shown in Fig. 4 is critical for the successful capture of RLV. For the current study, the ACCD is 2 m long with a cross-sectional diameter of 1.5 m. The four large fins, which can deflect up to a maximum of ±15° provide 6DOF agility and control. The nose of the ACCD is attached to the towing aircraft byvia rope and the back cone of the ACCD secures the connection with the RLV [5].

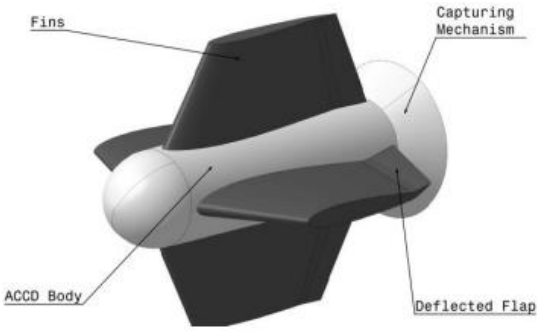


Fig. 4: ACCD Geometry [6].

## 3. Selection of the operational condition for the coupled simulation

Before setting up the coupled simulation, it is important to identify the operational conditions in terms of the AoA and the position of the coupled devices behind the wake of the TA.

### *3.1 Aircraft Wake*

During the formation flight, the RLV needs to be in the vicinity of the TA wake, up to about 350 m downstream. This might have an impact on the performance of the RLV leading to a loss of formation due to the disturbances caused by the wake of the TA. Another source of disturbance is the landing gear which causes additional vortices to form, thus, contributing to the wake turbulence. To investigate these phenomena, RANS calculations are performed of the TA with front and side landing gears deployed as well as spoilers at -20°. A more detailed description of the CFD simulations is provided in [5]. The velocity contour plots for 0° and 6° AoA given in Fig. 5 exhibit a wake deficit which is visible as far as 315 m from the nose of the TA. To have a better insight on the wake results, the wake velocity components in streamwise direction (horizontal) and downwash direction (vertical) as a function of distance from the TA is presented in Fig. 6. The magnitude of the streamwise velocity ($U_y$) remains similar for both AoA whereas the deficit drifts in the Z-direction due to the higher AoA [1]. On the other hand, the downwash component

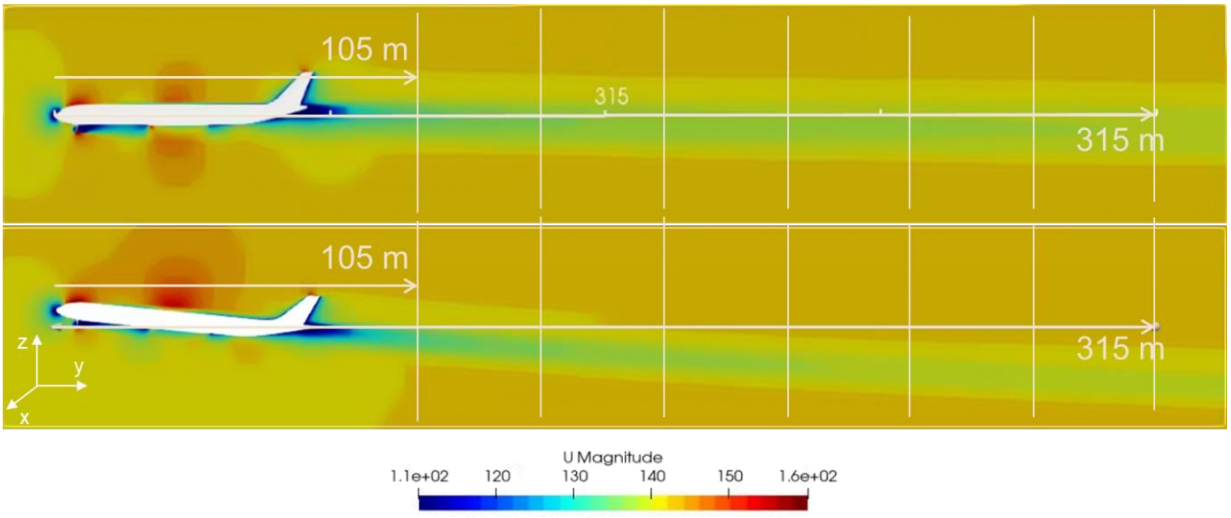


Fig. 5: 2D contour plot of the towing aircraft in the symmetry plane for two different angles of attack; 0° (top) and 6 ° (bottom) [5].

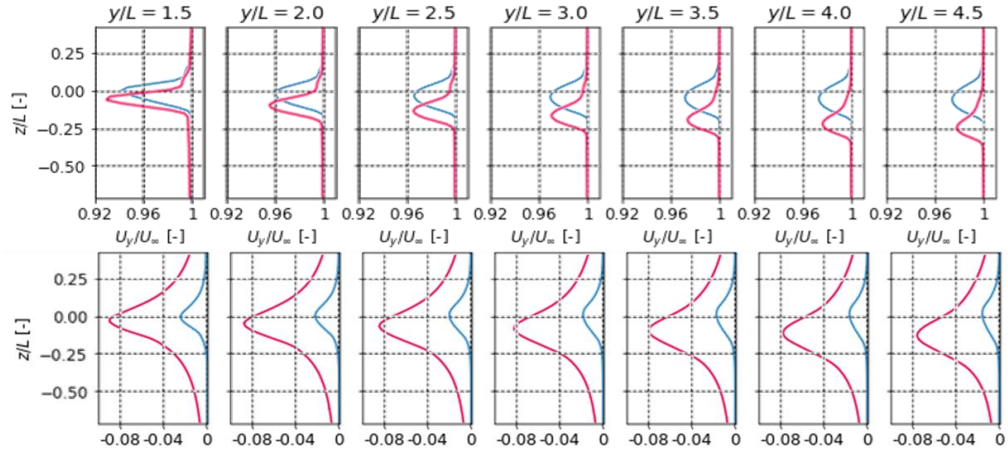


Fig. 6: Wake Profiles in the Fuselage Plane for 0° (blue) and 6° (red) AoA; Streamwise Velocity Component (top) and Downwash Velocity Component (bottom) [5].

($U_z$) is strongly dependent on the AoA as the magnitude increases with higher AoA. Moreover, $U_z$ remains almost constant along the wake region, remains close to 8% of the free stream velocity ($U\infty$) [1]. As the deficit caused by this component is strong and does not fade away, it can possibly affect the AoA of the RLV and prevent formation [1]. Moreover, the relative velocity field in the XZ plane extracted at 150 m behind the TA, which is shown in Fig. 7, exhibits the tip vortex formation. It should be noted that placing the ACCD within ±30 m in X direction and also between -20 m to 15 m in Z direction will introduce disturbances which will introduce disturbances that may destabilize the ACCD. Thus, it is critical to analyse the sensitivity of the formation flight trajectory to the wake disturbances.

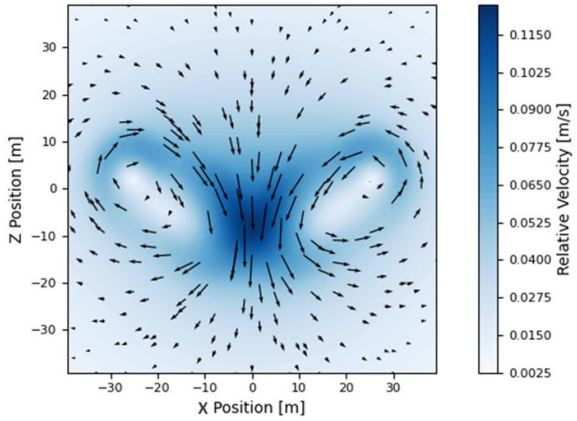


Fig. 7: Relative velocity in vector field from XZ plane.

*3.2 Wake disturbances*

As observed in Sec. 3.1, the aircraft wake at higher AoAs has a significant downwash component that can disturb the AoA of the RLV when exposed to it. For an AoA of 8°, this component was found to reach up to 11% of free stream velocity. Such a high deficit in vertical velocity can drastically disturb the formation and therefore, should be analysed. Fig. 8 shows the preliminary simulations performed in formation flight inserting the wake profile as inlet boundary condition. It appears that the RLV is being exposed to the wake (highlighted by the orange shaded region) up to 50% of the capture window (highlighted by the green shaded region). This causes major disturbances in the AoA of the RLV leading to a reduction in formation envelope by approximately 10 s. Since the end goal of the ACCD is to capture the RLV during this capture window, the influence of the wake on the mated configuration should not be overlooked. Disturbance in AoA of the mated configuration may also lead to some flow separation phenomena at higher AoAs which should be analysed. Therefore, for the CFD calculations, the mated configuration is defined such that the RLV coupled to the ACCD are exposed to the wake of the TA at a high AoA of 10°. The A340 is also expected to be at a similar AoA such that it generates sufficient drag to slow down to the velocity required for the capture envelope and to maintain a prolonged duration of formation flight. This subsequently exposes the downstream vehicles to a wake with a high AoA, that results in a strong downwash component.

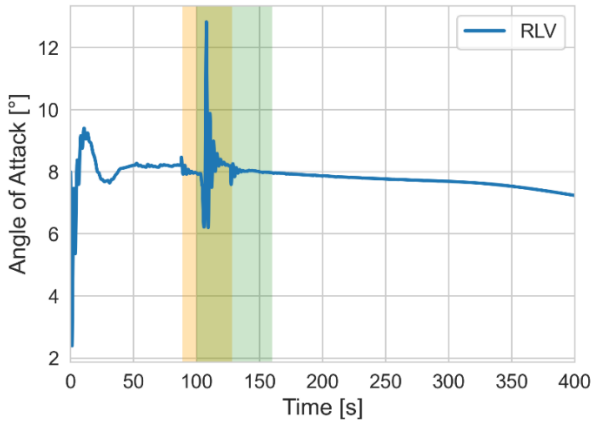


Fig. 8: Effect of Wake on RLV AoA during Formation Flight [1].

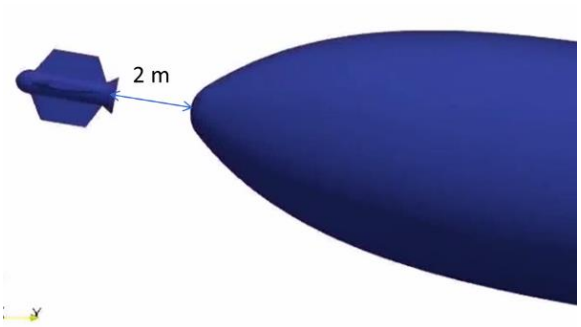


Fig. 9: Representation of the distance between the ACCD and RLV.

A fixed distance of 2 m is defined between the ACCD and RLV as a projection of the boom on to which the ACCD attempts to attach, as shown in Fig. 9. Fig. 10 shows the position of the two downstream vehicles in the wake of the aircraft. The horizontal separation between the two vehicles is based on the approximate horizontal distance at which the RLV crosses the wake in the preliminary simulations of the individual vehicles, as well as the length of the rope attached to the ACCD which is 225 m. Additionally, the distance

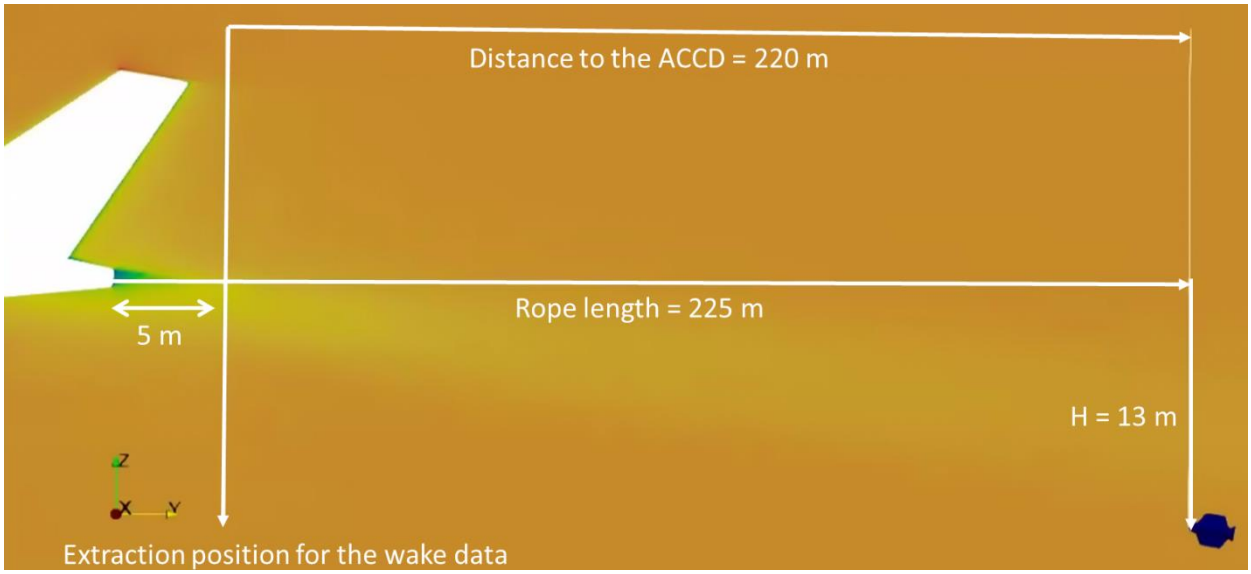


Fig. 10: Schematic placement of the coupled configuration with the location of the extraction plane.

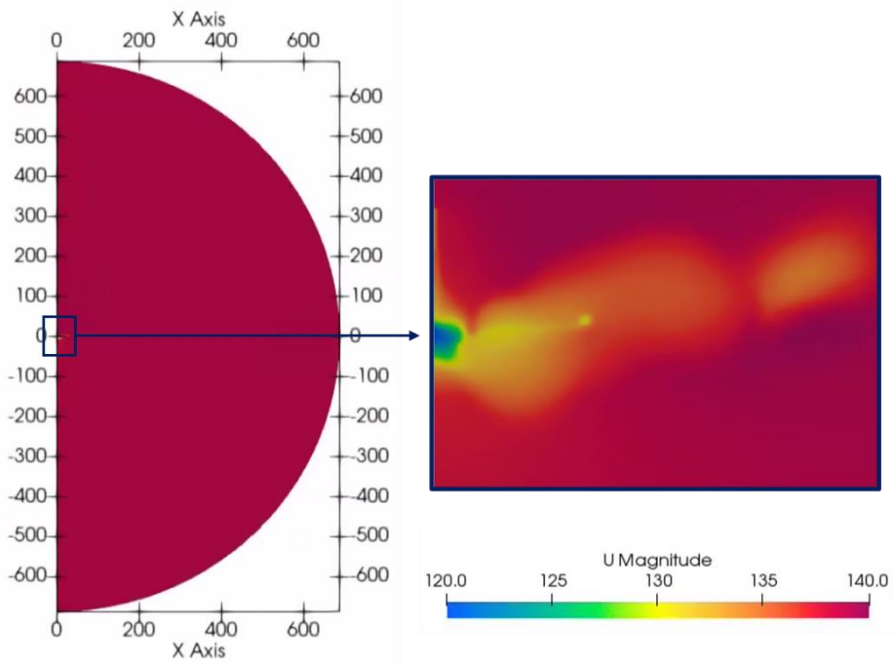


Fig. 11: Velocity magnitude of the wake extraction plane (left) and zoomed version (right).

H is selected to be 13 m below the reference to expose the two vehicles to the strongest downwash component and therefore, analyse the unmitigated effects of the wake on the coupled vehicles.

## 4. Computational domain

The size of the computational domain for the coupled simulation is chosen such that the aircraft wake from the previously performed simulation can be imposed as an inlet boundary condition. The wake data is extracted right after the towing aircraft by considering the rope length determined by DLR (see Fig. 10 for the extraction location). The wake extraction plane shown in Fig. 11 is then imported as inlet boundary condition for the coupled simulation. Even though the extraction plane is a half-circle the upper and lower extremities of the domain is uniform, thus, interpolation of the inlet field to a rectangle is not introducing additional spurious errors.

The upstream distance from the coupled vehicles is determined by the difference between the location of

the wake extraction plane and the rope length as shown in Fig. 11. The upper and the bottom parts of the domain are determined by the wake extraction plane and verified to have enough distance from the devices to avoid the arbitrary reflections. The overall representation of the computational domain is given in Fig. 12 with a domain size of 4l and 18l in the upstream and downstream directions, respectively while the wall normal direction is 12l where l is the RLV's fuselage length (60 m). The half domain (symmetry) approach is applied to reduce the computational cost.

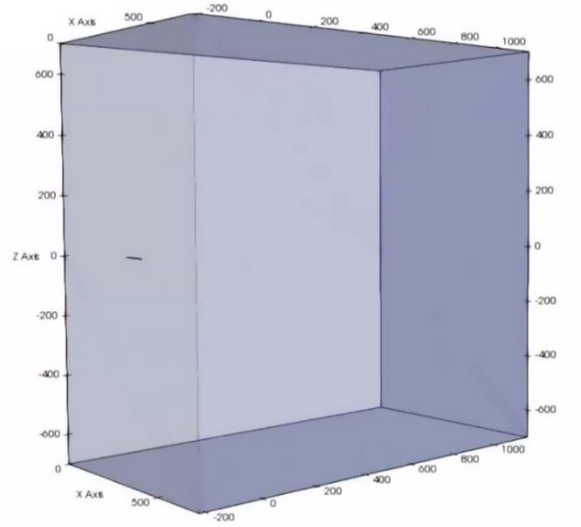


Fig. 12: Computational domain.

## 5. Computational setup

Steady-state three dimensional (3D) compressible RANS simulations are performed with the open source CFD solver OpenFOAM 6.0 using the k-ω SST turbulence model and rhoSimpleFoam solver. A half domain with a symmetry boundary condition applied to the central plane is used to reduce the mesh size and therefore reduce the computational cost by two. For the boundary conditions, the configuration given in Table 1 is used. The inletOutlet boundary condition provides a generic outflow condition, with specified inflow for the case of return flow while the freeStream boundary condition provides a free-stream condition. It is a "mixed" condition derived from the inletOutlet condition, whereby the mode of operation switches between fixed (free stream) value and zero gradient based on the sign of the flux. The inlet boundary conditions are imposed as a table where the points are interpolated according to the new mesh.

## 6. Mesh generation

The mesh is created with snappyHexMesh, which is a mesh generation utility of OpenFOAM, consisting of hexahedra (hex) and split-hexahedra (split-hex) cells with an option of boundary layer cells insertion on the surfaces. The final mesh parameters which were selected during the mesh sensitivity analysis in [8] are applied here. Since the inlet boundary condition is not uniform in this case, a coarser mesh cannot be used for the wake zone. Thus, an additional wake refinement box (see Fig. 13) must be added to capture the main wake features of the original wake data without focusing on the small features, which increases the computational efforts. The comparison between the original wake data and the imposed data is given in Fig. 14, shows that the coarsest cell size of the original wake data (upper right extremities) is selected for the refinement box. Moreover, this refinement box is extended before and after the coupled devices for two purposes. The first one is again to keep the wake features till the ACCD and the latter is to well define the wake properties of the RLV (see the refinement box in Fig. 13.)

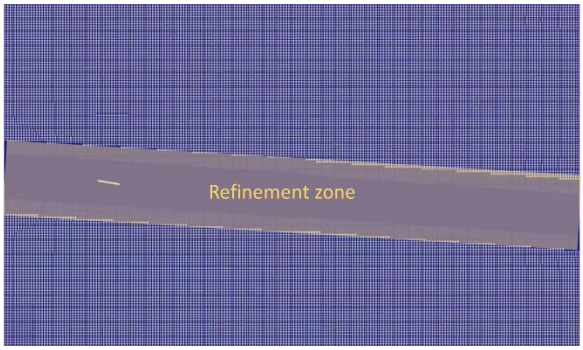


Fig. 13: Refinement zone for the wake region.

Table 1: Boundary conditions.

| | U [m/s] | p [Pa] | k [m2/s2] | ω [s-1] | T [K] |
|---|---|---|---|---|---|
| **Upper & bottom** | Freestream velocity | Freestream pressure | inletOutlet | inletOutlet | inletOutlet |
| **Outlet** | Freestream velocity | Freestream pressure | inletOutlet | inletOutlet | inletOutlet |
| **Bodies** | No slip | ∇p=0 | Wall Functions | Wall functions | ∇$T$=0 |
| **Freestream values** | Imposed as a table in the boundary condition | | | | |

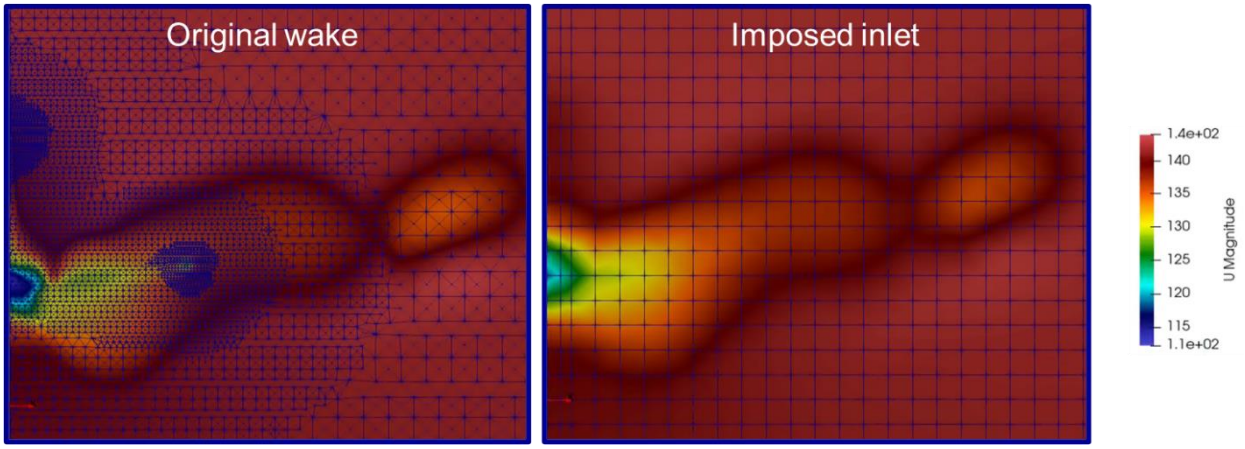


Fig. 14: Wake plane from A340 simulation (left) and the inlet coupled simulation plane (right).

## 7. Results and discussions

The magnitude and the downwash component of the velocity field are given in Fig. 15 and Fig. 16, respectively. From the figures, it is clearly observed that the wake pattern in the downstream direction, wake slope, is changing significantly depending on the velocity component. Even though when the magnitude of the velocity is considered, the ACCD and RLV are not exactly downstream of the wake deficit while the downwash velocity component demonstrates that they are placed exactly on the wake deficit as described previously. Due to strong downwash velocity component, the effective AoA of the ACCD and RLV are expected to be lower than 10°. The effective angle of attack of the ACCD is calculated by considering only the streamwise and downwash velocity component. Since the incoming flow-field is not uniform, these values are taken upstream of the ACCD where the flow-field is not affected by the presence of it. The effective AoA is found to be between 5°- 6° as the downwash velocity is varying along the z direction which could be seen clearly in Fig. 16..

The interaction between the ACCD and RLV is analysed by plotting the streamlines as shown in Fig. 17. The formation of two counteracting asymmetric vortices is observed in the wake of the ACCD. This

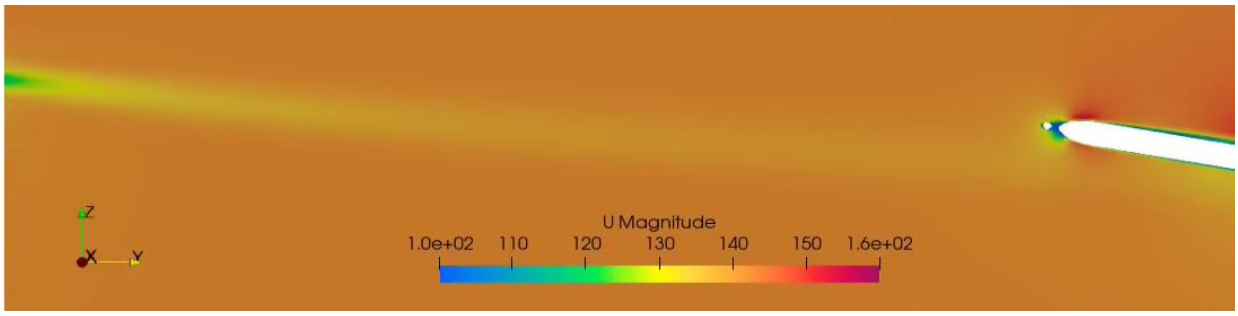


Fig. 15: Magnitude of the velocity field in YZ plane.

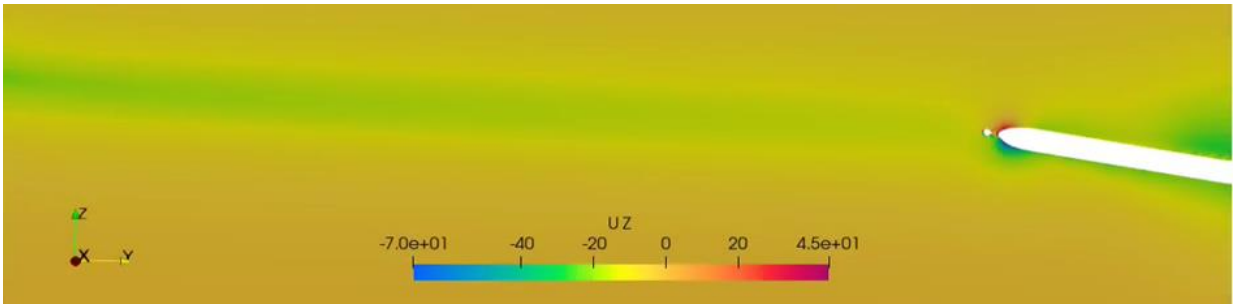


Fig. 16: Downwash component of the velocity field in YZ plane.

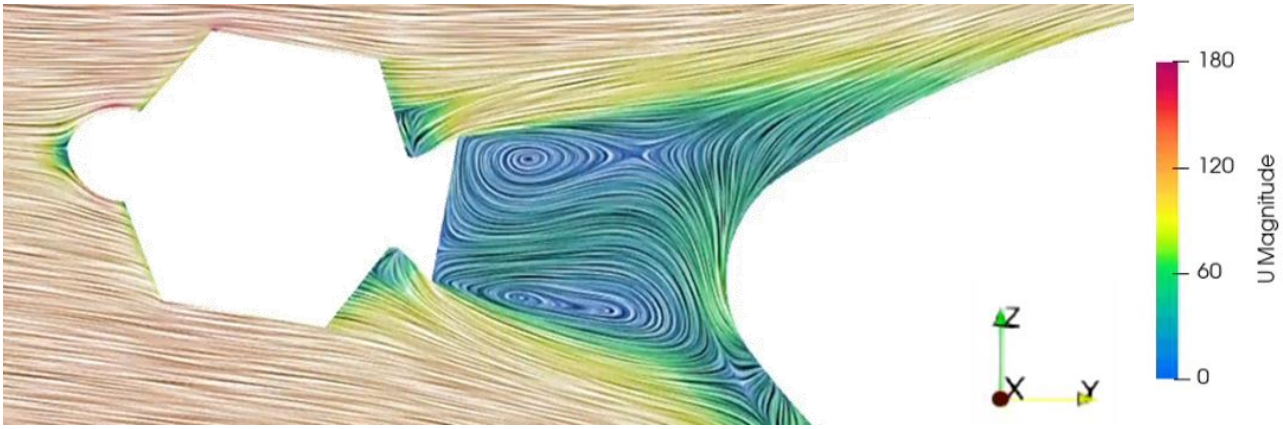


Fig. 17: Close view of vortex formation behind the ACCD in coupled case.

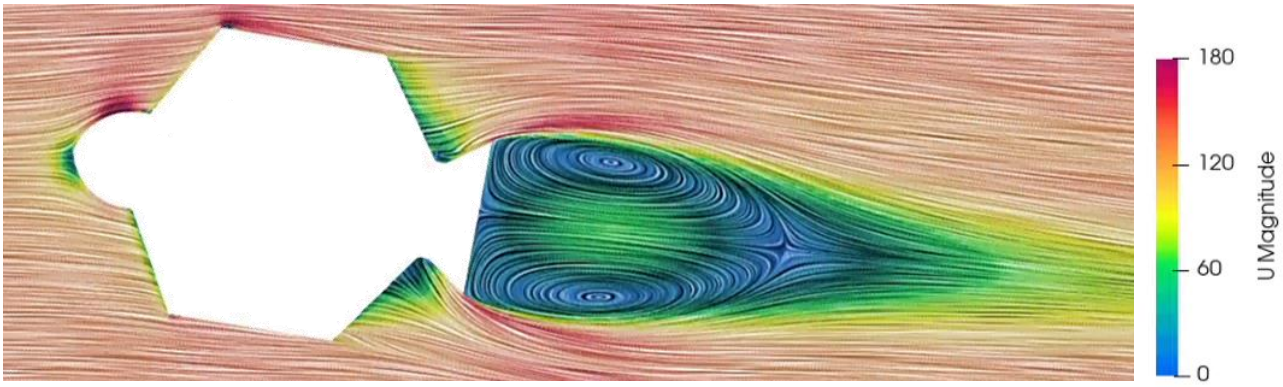


Fig. 18: Close view of vortex formation behind the ACCD in alone case at 10°.

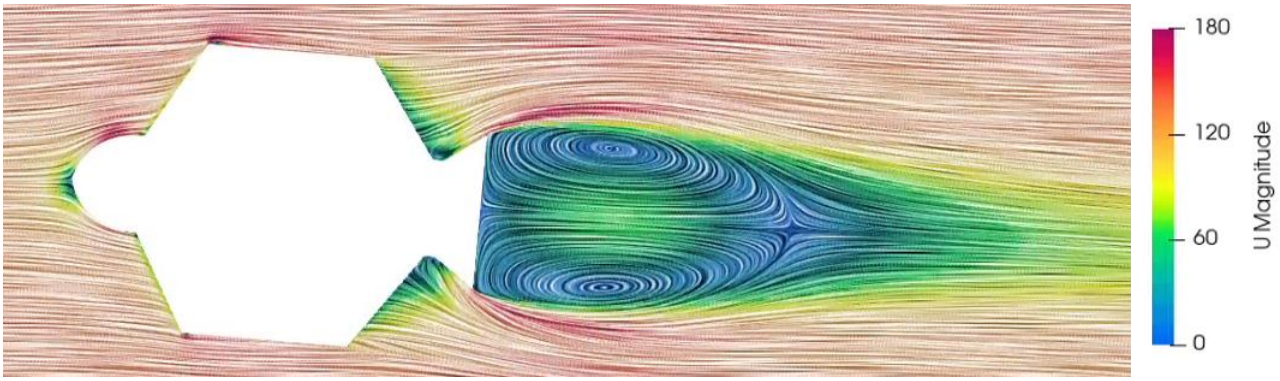


Fig. 19: Close view of vortex formation behind the ACCD in alone case at 5°.

might be due to the non-uniform flow field or the presence of the RLV. When comparing the flow-field with the undisturbed flow simulations of the ACCD alone at the same geometrical AoA, 10° (see Fig. 18), it is observed that the velocity magnitude on the upper part of the nose and the leading edge of the wing are found to be higher compared to the coupled simulation due to the non-uniform inlet velocity which is lower. Moreover, the wake formation behind the ACCD is not fully completed due to the presence of the RLV and the streamlines are following the body of the RLV rather than following the freestream velocity as in the case of the ACCD alone, thus, having a wider wake. The recirculation zones are found to be smaller than the ACCD alone case. The comparison in terms of the effective AoA, 5°, is be found in Fig. 19 where no significant difference is observed on the wake formation except the lower velocity behind the ACCD due to the lower AoA. Furthermore, the stagnation point on the nose of the RLV is also responsible for the

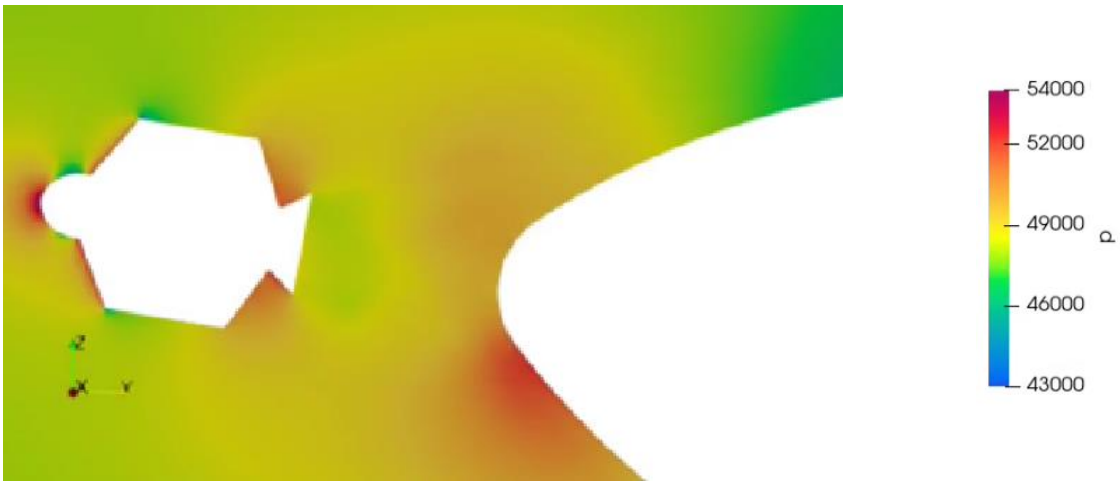


Fig. 20: Close view of the pressure field for the coupled simulation.

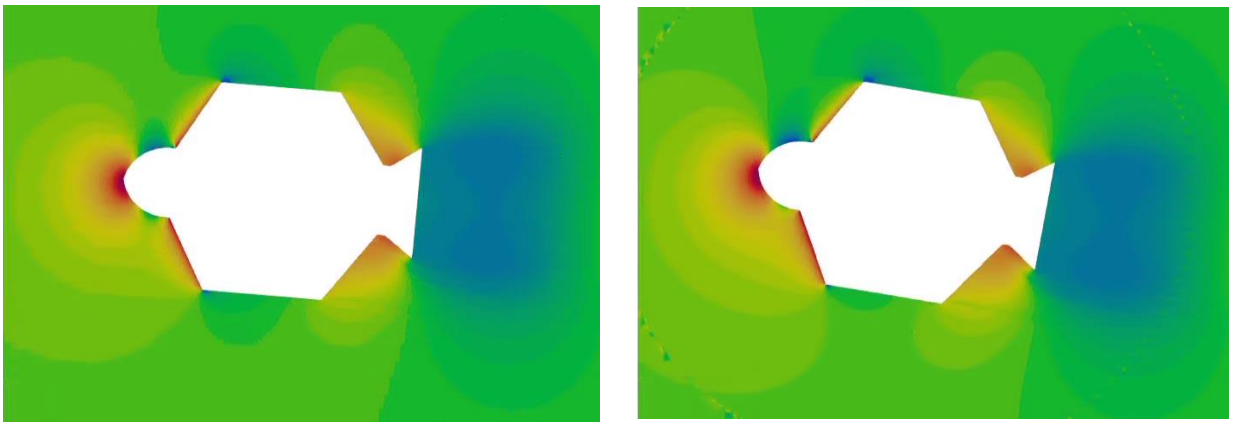

Fig. 21: Close view of the pressure field for the ACCD alone simulation at 5° (left) and 10° (right).

increase in pressure in the wake of the ACCD. As a result, not only the pressure field behind the ACCD but also around the ACCD is found to be higher compared to the one of the ACCD alone simulations as seen in Fig. 20 and Fig. 21. Since the flow field is significantly affected by the presence of the RLV and the downwash component of the velocity, it is also expected to obtain different aerodynamic coefficients in this coupled simulation. The lift and drag coefficient for ACCD and RLV are given in Table 2 and Table 3 with their respective standard deviation as it has been found that the flow field has an unsteady nature, thus resulting in an oscillating behavior. In this procedure, the last time steps where the oscillating behavior is observed are averaged and the standard deviation is calculated. The lift of the ACCD in the coupled simulation is found to be 2.8 times lower than the alone simulations at the same geometrical AoA while a better prediction (1.3 times lower) is established with the effective AoA, On the other hand, the drag coefficient is found to be lower in comparison with the effective AoA case since the size of the wake, thus, the pressure losses are higher in the ACCD alone case which increases the pressure drag. The aerodynamic coefficients of RLV in the coupled simulation is compared with the RLV alone simulations in the undisturbed flow [7] and concluded that the downwash velocity component and the presence of the ACCD did not affect the results as significantly as ACCD which is expected as the ACCD is 30 times smaller than the RLV allowing it be affected by small disturbances.

Table 2: The comparison of the aerodynamic coefficients of the ACCD.

| **ACCD** | | | | |
|---|---|---|---|---|
| | Cl | | Cd | |
| Simulation | Mean | Sd | Mean | Sd |
| Coupled | 0.3 | 0.35% | 0.2 | 0.16% |
| Alone at 10° | 0.83 | - | 0.51 | - |
| Alone at 5° | 0.39 | - | 0.45 | - |

Table 3: The comparison of the aerodynamic coefficients of the RLV.

| RLV | | | | |
|---|---|---|---|---|
| | Cl | | Cd | |
| Simulation | Mean | Sd | Mean | Sd |
| Coupled | 3.36 | 1.23% | 0.59 | 1.44% |
| Alone at 10° | 4.34 | - | 0.47 | - |
| Alone at 6° | 2.98 | - | 0.33 | - |

## 8. Conclusions

This paper has covered the aerodynamic CFD analysis performed by VKI on the coupled simulation in diving configuration. Instead of performing three vehicles in diving configuration, the simulation is divided into two steps. The first one is to perform the towing aircraft simulations alone to obtain the wake field. The second step is to simulate the ACCD and RLV together by imposing the wake data obtained from the towing aircraft simulation at the inflow.

The mesh parameters and the computational setup are selected based on the previous studies reported in [8]. The computational domain is chosen as a rectangular box instead of a cone shape to perfectly project the wake data of the towing aircraft simulation at the inlet of the domain. The positioning of the ACCD and RLV is determined by the analysis performed by DLR and chosen to be the horizontal distance from the nose of the aircraft as 295 m, the vertical distance as 13 m below the reference to place the configuration, and a fixed distance of 2 m is defined between the ACCD and RLV. The AoA of the ACCD and RLV is 10° and the imposed wake data configuration is chosen to be 10°. The simulation results show that the downwash velocity component is changing the effective angle of attack seen by the ACCD and RLV. Even though the devices are positioned at a higher AoA, the effective AoA would be lower due to the downwash component. This will also reduce the drag and lift coefficients as the AoA is reduced and brings the ACCD further away from the stall region. Moreover, it is observed that the presence of the RLV is changing the flow field significantly when compared to the ACCD alone simulation. Two counteracting asymmetric vortices are observed due to the non-uniform flow conditions, which may also be due to the placement of the RLV which is not perfectly aligned. The ACCD wake region is found to be shorter, and the pressure is higher than the ACCD alone case due to the flow interactions with the RLV. The aerodynamic coefficients are presented for each device with their standard deviation as the flow field is unsteady by nature, for consideration in the flight dynamic simulations by DLR.

## Acknowledgements

This work was performed within the project '**F**ormation flight for in-**A**ir **L**auncher 1st stage **C**apturing demonstrat**ion**' (**FALCon**) addressing development and testing of the "in-air-capturing" technology. FALCon, coordinated by DLR-SART, is supported by the EU within the Horizon2020 Programme 5.iii. Leadership in Enabling and Industrial Technologies – Space with EC grant 821953. Further information on FALCon can be found at http://www.FALCon-iac.eu

## References

[1] S. Singh, S. Stappert, L. Bussler, M. Sippel, S. Buckingham and C. Kucukosman, "A Full-Scale Simuation and Analysis of Formation Flight during In-Air-Capturing," 72nd International Astronautical Congress, Dubai, 2021.

[2] S. Singh, M. Simioana, S. Stapper, M. Sippel, S. Buckingham, S. Lopes and Y. C. Kucukosman, "Control Design and Analysis of a Capturing Device Performing In-Air Capturing of a Reusable Launch Vehicle," in *9th European Conference for Aeronautics and Space Sciences (EUCASS)*, 2022.

[3] S. Stappert, J. Wilken, L. Bussler and M. Sippel, "A Systematic Assessment and Comparison of Reusable First Stage Return Options," in *70th International Astronautical Congress*, 2019.

[4] M. Sippel, S. Stappert, L. Bussler, S. Krause, S. Cain, J. Espuch, S. Buckingham and a. V. Penev, "Highly efficient RLV-return mode "In-Air-Capturing" progressing by preparation of subscale flight tests," in *n 8th European Conference For Aeronautics And Space Sciences (EUCASS)*, 2019.

[5] S. Singh, S. Stappert, S. Buckingham, S. Lopes, Y. Kucukosman, M. Simioana, M. Pripasu, A. Wiegand, M. Sippel and P. Planquart, "Dynamic Modelling and Control of an Aerodynamically Controlled Capturing Device for 'In-Air-Capturing'," in *11th International ESA Conference on Guidance, Navigation & Control Systems*, 2021.

[6] S. Singh, L. Bussler, S. Stappert, S. Callsen, M. Sippel, S. Lopes and S. Buckingham, "A Superposition Approach to Aerodynamic Modelling of a Capturing Device used for In-Air Capturing of a Reusable Launch Vehicle," in *9th European Conference for Aeronautics and Space Sciences (EUCASS)*, 2022.

[7] S. Singh, L. Bussler, S. .. Stappert, M. Sippel, Y. C. Kucukosman and S. Buckingham, "Simulation and Analysis of Pull-Up Manoeuvre during In-Air Capturing of a Reusable Launch Vehicle," in *9th European Conference for Aeronautics and Space Sciences (EUCASS)*, 2022.

[8] Y. C. Kucukosman, S. Lopes, S. Buckingham, P. Planquart, S. Singh, L. Bussler, S. Stappert and M. Sippel, "Aerodynamic Characterization of In-Air Capturing Vehicles Using CFD Simulations," in *9th European Conference for Aeronautics and Space Sciences (EUCASS)*, Lille, 2022.

[9] M. Sippel, S. Stappert, L. Bussler and C. Messe, "Powerful and Flexible Future Launchers in 2-or 3-stage Configuration," in *70th International Astronautical Congress*, 2019.

[10] E. J. Saltzman, "Aerodynamic Assessment of Flight Determined Subsonic Lift and Drag Characteristics of Seven Lifting-body and Wing-body Reentry Vehicle Configurations," Dryden Flight Research Center, 2002.

[11] "A340-600 Global Performer, Previous Generation Aircraft," [Online]. Available: https://www.airbus.com/aircraft/previousgeneration-aircraft/a340-family/a340-600.html. [Accessed 2022].

[12] M. Sippel and J. Klevanski, "“Progresses in simulating the advanced in-air-capturing method," in *5th International Conference on Launcher Technology, Missions, Control and Avionics*, 2003.

[13] R. Martinez-Val, E. Perez and J. F. Palacin, "Historical Evolution of Air Transport Productivity and Efficiency," in *43rd AIAA Aerospace Sciences Meeting and Exhibit*, 2005.